Environ Earth Sci (2015) 74:3207–3221
DOI 10.1007/s12665-015-4358-y

ORIGINAL ARTICLE

Deterioration mechanisms of the compact clay-bearing limestone of Tournai used in the Romanesque portals of the Tournai Cathedral (Belgium)

Laurent Fontaine[1] · **Roel Hendrickx**[1] · **Hilde De Clercq**[1]

Received: 6 November 2014 / Accepted: 26 March 2015 / Published online: 7 April 2015

Abstract Tournai stone has been extensively used in Western European historical architecture and is subjected to severe deterioration mechanisms, which were investigated in two Romanesque portals of the cathedral of Tournai city. The stone material was studied with thin-section petrography and SEM-EDX and its hygric, hydric and thermal properties were measured. The porosity is very low and the pore size distribution can be related to either typical pores associated with the clay fraction or with micro-cracks. The formation and propagation of cracks are related to anisotropy of the stone (clay presence in laminae with a preferred direction) and the influence of different external climatic factors. As expected, the effect of liquid water has the highest damage potential while the clay fraction imparts a pronounced hygroscopic behaviour to the stone. The identified clay mineral was illite. Although its non-swelling properties exclude interlayer swelling as a cause of damage, interparticular osmotic pressure is recognized as the most plausible damage cause at the micro-scale. Gypsum crusts occur in two morphologies: films and thick deposits, both showing a comparable layered structure, but significantly differing in the proceeding process and shapes and features. Due to the nature of the stone and of the damage processes, feasible measures for preventive conservation on the long term are to be found in the direction of decreasing the climatic influence by means of sheltering.

✉ Laurent Fontaine
laurent.fontaine@kikirpa.be

[1] Monuments Laboratory, Royal Institute for Cultural Heritage (KIK-IRPA), Parc du Cinquantenaire 1, 1000 Brussels, Belgium

Keywords Tournai stone · Delamination · DRMS · Capillary absorption · Dilatation · Black crusts

Introduction

The construction of the Cathedral of *Notre-Dame* (Our Lady) in Tournai (Belgium) started in the first half of the twelfth century. Its nave and transept date back to the Romanesque period and are topped with five towers, all predating the Gothic choir. In recognition of its important artistic and historic value, the Cathedral was designated by UNESCO as a World Heritage Site in 2000. Despite the successive architectural changes of the Romanesque construction, two original side portals were spared: the *Mantile* and *Capitole* portals, located, respectively, at the NE and SE side of the nave and dating back around 1125 (Delé-houzée 2013). These finely sculpted portals represent unique examples of Romanesque monumental sculpture in Western Europe, in spite of their strongly deteriorated state.

The Mantile and Capitole portals were executed in black Tournai stone, a local "marble" (sedimentary limestone able to take a good polish), which was widely used in the Low Countries from the eleventh to the fifteenth century (Groessens 2008). Renowned for its deep black gloss, black Tournai stone was exported to England (Drake 2002) and even to Scandinavia (Storemyr et al. 2007). Geologically, the black Tournai stone is a compact, fine-grained, silicified and clay-bearing limestone of Lower Carboniferous (Tournaisian) age (Camerman 1944; Hennebert and Doremus 1997).

After a heavy thunderstorm in 1999, the need for a new restoration campaign of the whole monument was considered crucial. In this framework, a preliminary study of the

Romanesque side portals was commissioned in 2012 by the Walloon cultural heritage agency (*DGO4/Département du Patrimoine*), the *Province of Hainaut* and the *City of Tournai* aiming to understand the deterioration mechanism(s) of the black Tournai stone in an urban environment to formulate recommendations for a long-term conservation strategy of the portals.

Materials and methods

Petrographic examination and identification of the clay fraction

Four minor stone samples were taken from the portals for detailed petrographic investigation by means of thin sections. One sample was lifted from a compact stone core while three others from outer edges of the ashlars. A polarizing microscope (Axioplan, Zeiss) was used, equipped with a high-resolution digital camera (DeltaPix Invenio 5DII). Additionally, four samples of black crusts (films and thick deposits) were taken from the portals and subjected to an analysis by thin-section petrography (polarized light microscopy) and scanning electron microscopy coupled with an energy dispersive X-ray spectrometer (SEM-EDX).

According to literature, the clay content of the stone is about 8 % on average (Camerman 1944; Hennebert and Doremus 1997). To identify the type of clay mineral(s) present in the stone, X-ray diffraction (XRD) analyses were performed on the clay fraction (particle size <2 μm) of three samples from the Capitole portal, with a Philips Analytical X-ray B.V. The clay fraction of each sample is further subdivided into 3 parts which were subjected to a different conditioning: (1) treatment by heating at 490 °C, (2) treatment by ethylene glycol saturation during 12 h, and (3) no specific treatment (natural). Treatments 1 and 2 generate diagnostic modifications of the interlayer space in the case of swelling clay minerals. The extraction method of the clay fraction, as well as details of the analytical procedure, is described in Holtzapffel (1985).

In situ measurements

In a first phase of the research, a detailed visual inspection of both portals has been carried out from scaffoldings. A full mapping was made of the direction of the stone's stratification and its apparent pathology.

To characterize the deterioration degree in depth of the stone, twenty-seven hardness profiles were recorded with a micro-drilling resistance device (Drilling Resistance Measurement System of SINT Technology), using the default parameters (penetration rate 10 mm/min, revolution speed 600 rpm) and a 4.8 mm drill bit with "flat" diamond top provided by SINT.

The dynamic modulus of elasticity (E_{dyn}) was determined from the ultrasonic pulse velocity in direct transmission mode (UPV_{dir}), measured by means of a BP-5 device of UltraTest (Steinkamp) equipped with exponential (conical) probes. The measurements were performed in situ on stone elements of both portals (1) and, as comparison, on corner ashlars of the north transept (2), as well as on fresh blocks (sawed and carved) commissioned for restoration works at the south nave (3). The velocity (V, ms^{-1}) is obtained by the ratio of the distance between the transmitter and receiver transducers to the travel time through the material. The E_{dyn} (GPa) is then calculated from the following formula (Siegesmund and Dürrast 2011):

$$E_{dyn} = \rho V^2 \frac{(1+v)(1-2v)}{(1-v)}$$

where ρ is the bulk density [2665 kg m^{-3} based on the technical sheet of the Belgian Building Research Institute (CSTC 1986)] and v the Poisson's ratio (0.20 as default value).

Water absorption measurements were performed both in situ and in the laboratory. For in situ tests, a Karsten tube was used according to a procedure described in Hendrickx (2013). This method consists in a continued follow-up of the uptake as a function of time, and a further treatment of the data allows an interpretation in terms of sorptivity and capillary saturation water content.

Capillary water absorption and porosimetry

Laboratory measurements of capillary water absorption were performed on 8 prisms (2 × 2 × 4 cm) cut from original blocks from the nave, which were discarded at the time of restoration. Blocks showing visible stratification and various deterioration degrees were selected to dispose of samples representative of those in the portals. Four prisms have their length parallel to the bedding, while four others perpendicular to it. The test consists of unidirectional capillary absorption in the vertical direction through the bottom face of the prisms, which was put in contact with distilled water. The lateral faces were sealed with tape. The mass increase was recorded during 32 h.

The porosity and the pore size distribution were characterized by mercury intrusion porosimetry (MIP), using a Micromeritics Autopore IV apparatus. Because of the low porosity and the probable presence of nano-pores, a 5-min long equilibration time was adopted for each intrusion step.

Hygroscopic moisture uptake

To quantify the hygroscopic moisture uptake, 30 prisms (2 × 2 × 4 cm) cut from original blocks from the nave were oven-dried at 60 °C to constant weight and then stored at 20 °C and 95 % relative humidity (RH) in a climatic chamber. The mass increase was registered after 28 and 56 days. The hygroscopic moisture content (HMC_{95}) was calculated as the mass increase relative to the dry mass.

Dilatometry

Thermal, hygric and hydric dilatation measurements were carried out on a series of prisms (2 × 2 × 4 cm) cut from original blocks from the nave. A holder ("dilatometer") for 3 samples was custom-designed in Invar (Fig. 1), a nickel–iron metal alloy characterized by a low coefficient of thermal expansion (α in the order of 1.2×10^{-6}/K). For hygric and thermal cycling, the whole setup was placed in a climatic chamber (Heraeus/Vötsch). Sample deformation during cycling was measured by means of high-resolution digital displacement transducers (Solartron) with an accuracy of 0.20 μm.

Thermal cycles consist of 3 h at a low temperature of 10 °C, a linear increase to 60 °C during 1 h, constant high temperature during 3 h and a linear slope down again to 10 °C during 1 h. The total cycle takes 8 h during which the RH was kept constant at 60 %. Two cycles were performed for each set of 3 samples. Pre-conditioning consisted of oven-drying at 60 °C for at least 24 h, followed by conditioning for 24 h at the initial set conditions.

Because the dilatometer itself is also heating up and cooling down, the measurements need to be calibrated to compensate for its deformation. Although the Invar frame has a relatively low expansion, this is not the case for the transducers, which are mainly made of aluminium, having a much higher α. Therefore, a reference measurement was carried out with quartz glass elements of approximately 10 cm length, a material with a well known and extremely low α. The results allow correcting the apparent obtained value for the dilatation related to the combination of frame and transducers.

Hygric cycles were performed at constant temperature of 20 °C. Each cycle starts at 40 % RH during 8 h followed by successively a linear increase to 80 % during 4 h, a plateau of 8 h at 80 % and a decrease back to 40 % over 4 h. Two consecutive cycles were performed for each set of 3 samples. Pre-conditioning consisted of oven-drying at 60 °C for at least 24 h, followed by conditioning for 24 h at the initial set conditions.

Apart from previous cycling, more or less representative of daily fluctuations in RH, three samples, previously conditioned during 56 days at 95 % RH, were submitted to a drastic decrease in RH to 40 %, hereby inducing a hygric shock.

Hydric expansion was measured by immersion of the samples in de-ionized water. For this purpose, a stainless steel container was inserted in the dilatometer. The samples were pre-conditioned at 20 °C and 50 % RH during at least

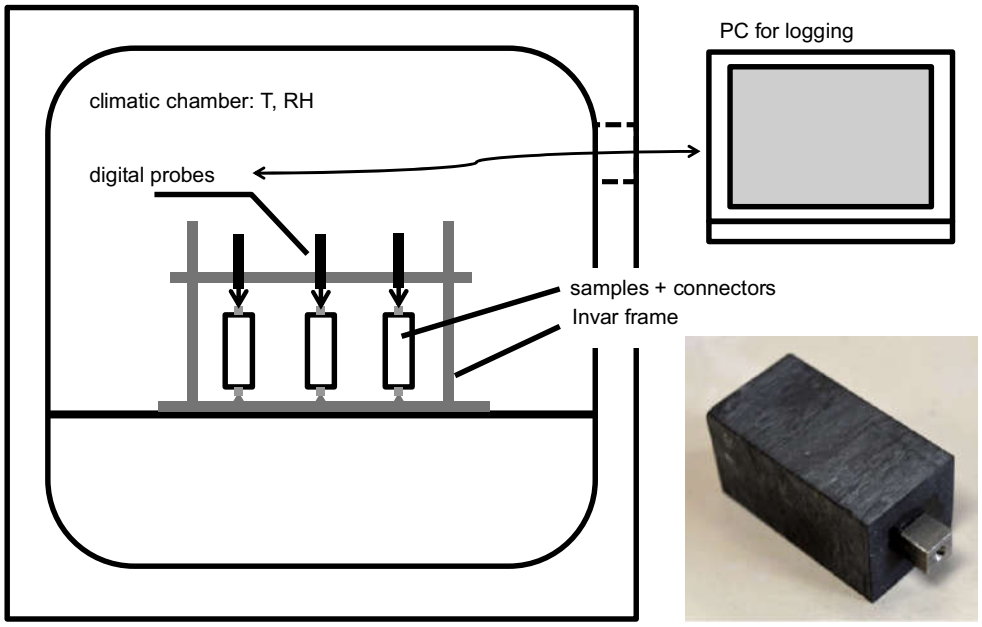

Fig. 1 Sketch of the dilatometer and close-up on a stainless steel extension piece mounted on a stone sample © KIK-IRPA (Monuments Laboratory)

4 h, after being oven-dried at 60 °C for at least 24 h. The temperature of 20 °C was kept constant, as was the water level in the container.

Preliminary tests showed that the positioning of samples between a smooth bottom plate and the tip of the displacement transducer led to horizontal movement of the samples during conditioning. For this reason, all samples were fitted with an epoxy-glued stainless steel extension at both ends (close-up on Fig. 1, bottom right). These extensions have a conical hole which fits a small stainless steel pointed or spherical connection piece of the dilatometer at the bottom and the tip of the transducer at the top, respectively.

Results and discussion

Concise description of the deterioration pattern

Detailed visual examination of the stone elements with the naked eye and a hand lens (×10) reveals a very fine-grained rock, with no macroscopically visible fossils or cherts. These features are typical for the lower part of the Antoing Formation and more specifically the Lower Calonne Member, which was historically used for numerous tombstones and baptismal fonts from the famous Tournai workshops (Nys 1993).

Generally speaking, the deterioration pattern of the Tournai stone consists of multiple delamination [i.e. detachments of flakes parallel to the bedding plane (ICOMOS-ISCS 2008)]. The bedding direction of the original blocks in both portals is represented in Fig. 2.

In the case of natural-bedded and edge-bedded stone blocks, the delamination process has caused an intense fragmentation in the outer edges; their schist-like appearance suggests a higher clay content compared to the compact stone core (Fig. 3). Face-bedded blocks suffer from material loss up to a few centimetres depth and, this to such a degree, that lots of sculpted reliefs are hardly readable (Fig. 4).

Two types of black crusts were identified: (1) more or less homogeneous films faithfully replicating the sculpted surface and (2) thick deposits of irregular thickness which disturb the reading of the underlying sculpted surface (Fig. 5).

The southwest orientation of the Capitole portal corresponds to the direction of prevailing winds and ample exposure to the sun. The deterioration degree of this portal is, therefore, higher than that of the Mantile portal and explains why more important restoration works in *Petit Granit* (also known as the "Belgian Bluestone") were carried out in the second half of the nineteenth century (Fig. 2a). Both types of black crusts are seen predominantly in zones sheltered from driving rain and water runoff.

Thanks to its northeast orientation, the Mantile portal is protected from wind and has little direct solar radiation. However, its location in an urban environment has led to extensive development of black crusts (Fig. 5). The severely damaged dripstone has stimulated rainwater running-off and hence biological colonization (green algae, mosses and lichens).

Stone characterization

The stone can be described as a bioclastic wackestone according to Dunham's classification (Dunham 1962) and

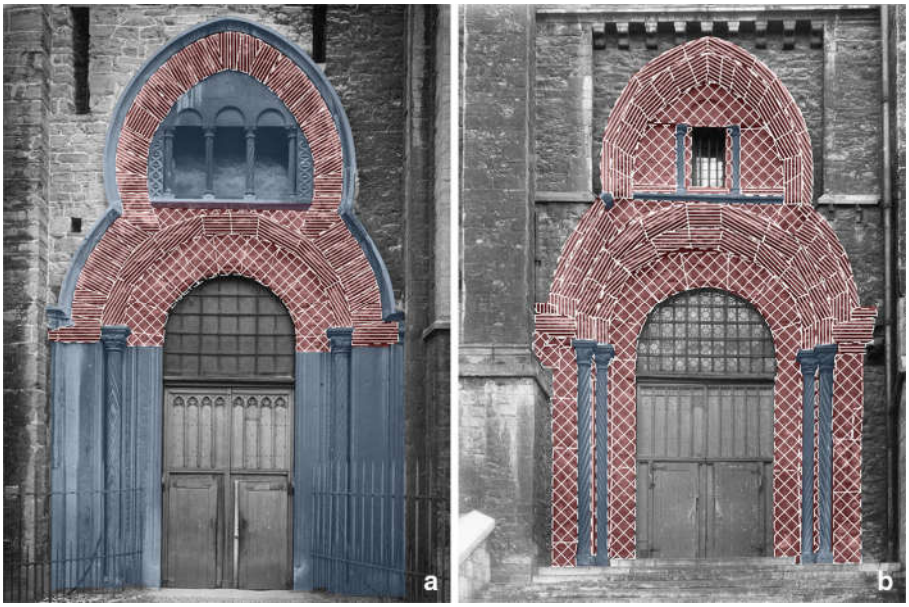

Fig. 2 Cartography of the bedding direction of the original stone blocks in the Capitole (**a**) and Mantile (**b**) portals. Hatching underlines the stone bedding, while crosshatching is used for face-bedded blocks. Blue-coloured zones correspond to restoration works in *Petit Granit* dating from the second half of the nineteenth century © KIK-IRPA (Stone Sculpture Workshop)

Fig. 3 Edge-bedded block displaying a compact stone core sandwiched by schist-like outer edges (Capitole portal, top of the trefoiled arch) © KIK-IRPA, Brussels

Fig. 4 Face-bedded block showing multiple delamination (Capitole portal, spandrel at the right side) © KIK-IRPA (Monuments Laboratory)

as a biomicrite according to the Folk's classification (Folk 1965). Petrographic features correspond with the descriptions of black Tournai stone found in the literature (Van Welden 1965; Dingelstadt and Dreesen 1996). XRD spectra on whole-rock samples and SEM-EDX mappings reveal that the silicified matrix of the stone is mainly made of calcite with, sometimes, grains of dolomite.

While the compact stone core (Fig. 6a) displays coarser bioclasts (≤250 μm) compared to the outer edges

Fig. 5 Summit of the Mantile portal. *Black* crusts (thick deposits), *green* algae, mosses and lichens can be identified © KIK-IRPA (Monuments Laboratory)

(≤100 μm) (Fig. 6b), careful examination reveals a more prominent presence of small clay laminae in these outer edges (Fig. 6d) which are almost absent in the stone core (Fig. 6c). The clay laminae impart a laminated structure to the outer edges of the stone.

While from microscopic investigation of the thin section of a compact stone core, no deterioration can be observed; the outer edges show the presence of numerous micro-cracks (width up to 250 μm) following the direction of the bedding or according to an angle up to 45° with it. This network of micro-cracks gives rise to a considerable fracture porosity, which was not present in the original rock material.

The spatial correlation between the clay laminae and the occurrence of micro-cracks suggests a strong causal link. Moreover, the pattern of micro-cracks is typical for stress-induced fractures in anisotropic materials, characterized by an alternation of zones with different elastic moduli (in this case: the calcitic groundmass versus the clay laminae).

The XRD spectra of the clay fraction show that the position of two characteristic peaks remains the same regardless of the type of conditioning, revealing the presence of non-swelling clay minerals. Peaks at 8.85 and 26.69°2θ correspond to basal spacings of 10 Å (d_{001}) and 3.33 Å (d_{003}), respectively, which are typical for illite. The absence of a peak around 17.7°2θ, indicative for the 5 Å (d_{002}) basal spacing of common illite, might reflect a relatively high iron content in the crystalline structure, as suggested by Esquevin (1969).

Micro-drilling resistance results (DRMS)

The overall of 27 DRMS measurements has shown that: (1) the compact stone core is characterized by a limited

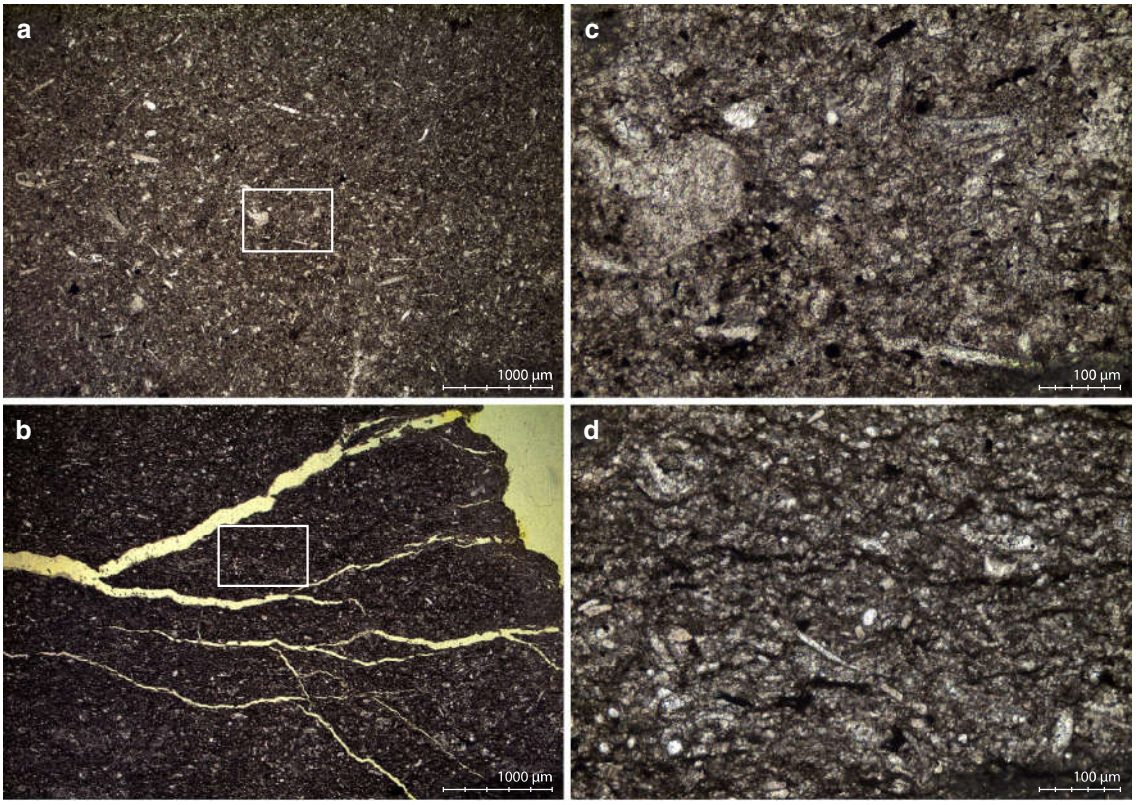

Fig. 6 Thin-section photomicrographs of *black* Tournai limestone from the portals. **a** General view in a compact stone core; **b** general view in an outer edge showing micro-cracks (*yellow*); **c** zoom in compact stone core (disseminated opaque grains correspond to pyrite); **d** zoom in outer edge (note the fine clay laminae in *black*) © KIK-IRPA (Monuments Laboratory)

weathering, with occasionally lower mechanical resistance zones (Fig. 7a); (2) significantly lower resistance and deeper weathering are noticed on slightly deteriorated outer edges (e.g. drill hole PC6), while the hardness of severely deteriorated outer edges (e.g. hole PM2) is reduced to 50 % and characterized by a pronounced noise reflecting a large number of micro-cracks (Fig. 7b); (3) face-bedded blocks present saw-tooth profiles corresponding to flakes and cracks (Fig. 7c); (4) thick black crusts have a lower drilling resistance than the underlying stone and can contain harder inclusions, corresponding to embedded stone fragments (Fig. 7d).

Young's modulus

Table 1 gives an overview of the results of UPV_{dir} and E_{dyn}. In fresh blocks, the E_{dyn} is mainly influenced by the direction of the bedding plane, which imparts anisotropy of the stone: values measured perpendicular to the bedding are significantly lower than those parallel to it. Compared to fresh blocks, the ones from the north transept show a 53 % decreased E_{dyn}, being, respectively, 40.3 and 19.1 GPa, which can be attributed to natural ageing during the centuries and/or a lower initial value. On the other hand, E_{dyn} of stone elements from both portals is primarily influenced by the state of deterioration. Going from a hard rock to a low cohesive material, the obtained values vary over 5 orders of magnitude. Stone elements with the lowest values can hardly fulfil any mechanical function: large cracks and block displacements might even affect the stability of the portals.

Hygric properties and description of the pore system

The execution of measurements with the Karsten tube in situ is very difficult, as surfaces are uneven and sometimes incoherent. Moreover, in the case of a stone in good condition, the absorption is very low and close to the detection limit of this technique. Nevertheless, a few measurements allowed to have a minimum of data about the actual water absorption behaviour of the stone material of the portals. The results are presented in the form of water uptake (ml) curves as a function of time. Water absorption data are then recalculated to an apparent value of the absorption coefficient according to the cited methodology. The value is only "apparent" because the validity of the method is strictly restricted to isotropic materials, while the stone is strongly anisotropic.

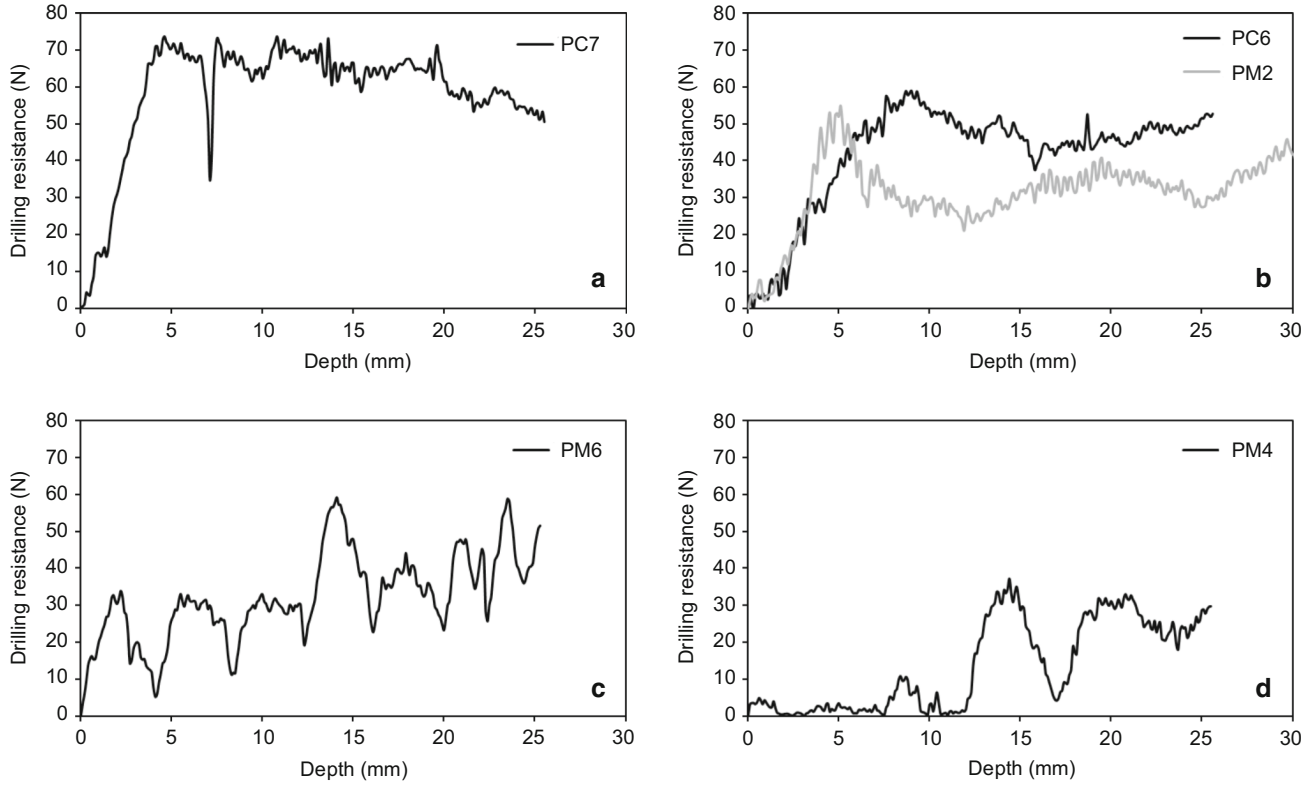

Fig. 7 Hardness profiles obtained on site by DRMS: **a** compact stone core (lower resistance at 7 mm); **b** deteriorated outer edges; **c** face-bedded block (note an increase of the hardness with depth); **d** edge-bedded block covered by a thick black crust up to 12 mm depth, then successively stone flake (12–17 mm) and deteriorated stone (from 17 mm) © KIK-IRPA (Monuments Laboratory)

Table 1 Overview of the UPV_{dir} and E_{dyn} (n is the number of measured samples per group)

	UPV_{dir} (m s^{-1})	E_{dyn} (GPa)
Elements of the portals ($n = 16$)		
Sound ($n = 2$)	5429; 6122*	69.8; 88.7*
Slightly deteriorated ($n = 7$)	1310 (473)	4.1 (3.8)
Severely deteriorated ($n = 7$)	312 (272)	0.3 (0.7)
Corners of the north transept ($n = 22$)		
Parallel to the bedding	2839 (1144)	19.1 (17.9)
Samples from blocks discarded during restoration of the nave ($n = 30$)		
Parallel to the bedding ($n = 12$)	4513 (1450)	48.2 (11.8)
Perpendicular to the bedding ($n = 18$)	3577 (891)	30.2 (15.3)
Fresh blocks for restoration ($n = 14$)		
Parallel to the bedding ($n = 9$)	4057 (885)	40.3 (17.3)
Perpendicular to the bedding ($n = 5$)	3812 (1546)	35.6 (39.3)

The stated values are mean values with the standard deviation between brackets when statistically relevant ($n > 2$), otherwise the measured values (*)

In analogy to the results for the Young's modulus, the variations in the capillary water absorption behaviour of the stone due to the deterioration degree are larger than those due to an execution according to a different direction of the bedding. In the case of slightly deteriorated stones, it proved very difficult to obtain meaningful curves: local defects in the stone (like deep cracks) caused significant deviations in the absorption. Such variations were relatively less important for the severely deteriorated stones.

Figure 8 illustrates a typical water absorption test executed parallel to the bedding (the bedding of the stone is

Fig. 8 Example of the formation of a wetted zone which is stretched to an ellipse shape in the direction of the bedding (dripstone of the Mantile portal) © KIK-IRPA (Monuments Laboratory)

perpendicular to the surface). Wetting occurs according to the orientation of the bedding. It can be assumed that the wet front does not have a hemispherical shape, as is expected in isotropic materials, but a half ellipsoid one with a long axis parallel to the bedding and a short one perpendicular to it. Absorption coefficients calculated from the results vary between 4 and 8 $g/m^2s^{0.5}$ for slightly deteriorated stones, while they can increase by a factor of ten for severely deteriorated ones (84 $g/m^2s^{0.5}$) (Table 2).

The restrictions related to in situ capillary water absorption tests on stones with widely varying characteristics were reduced by means of laboratory measurements: absorption is strictly unidirectional, sample size is exactly known, and environmental conditions are controlled. The results, presented in Fig. 9, show nevertheless that the average capillary uptake parallel to the bedding is much larger than the one obtained perpendicular to it. The mean absorption coefficients are 2.7 and 0.6 $g/m^2s^{0.5}$, respectively. Strong individual variations between samples of the same group can be attributed to differences in the deterioration degree. Samples from blocks 1 and 5 absorb faster and more than others, and those from block 6 rather slower and less.

The duration of the test was insufficient to determine a precise capillary saturation water content. However, the results of 2 samples which showed the fastest absorption (1a2 and 5a1) allow an estimation of the maximum water content of 1.7 and 3.2 vol %, respectively.

The average hygroscopic moisture uptake HMC_{95} was 0.6 vol %, which is in good agreement with the results of Lubelli and Nijland (2014) for fresh stone (0.5–0.6 wt%). The result is, as expected, not influenced by the bedding direction. This mass percentage corresponds to a volume percentage of 1.58 and represents, therefore, a considerable proportion of the maximum capillary water content (up to 3.2 vol %). This means that the stone's hygric behaviour is to a large extent determined by slow processes of hygroscopic moisture uptake. However, when deterioration becomes more severe, cracks induce a more pronounced capillary behaviour, being much faster, and hygroscopic behaviour becomes relatively less important.

Both capillary and hygroscopic water uptake are strongly linked to the pore structure. Fresh Tournai stone of good quality for construction is reported to have a very low porosity that virtually never exceeds 1 % (CSTC 1986). To characterize the secondary porosity, created by the process of micro-crack formation, 4 mercury intrusion porosimetry (MIP) measurements were performed on samples taken from original blocks from the nave. Samples 1, 2 and 5 correspond to stone fragments with increasing deterioration degree, while sample 4 represents a strongly fragmented schist-like outer edge. Results are presented in Fig. 10.

The measured total porosity varies from 1.6 to 4.2 vol %. However, these values have to be considered as a lower limit because the MIP technique does not allow a quantification of pores >0.3 mm (corresponding to large micro-cracks) or <80 nm. Although strong variations in cumulative porosity results are observed between the samples, a clear bimodal pattern in the pore size distribution can be discerned in all curves. A first pore family, situated between 0.01 and 0.8 μm, can be attributed to micropores between individual clay particles (inter-crystalline porosity). Indeed, sample 4, characterized by a considerable proportion of small-sized pores, was taken in a schist-like outer edge characterized by a high clay content. Situated beyond 100 μm, the second pore family is representative of the fracture porosity (micro-cracks observed in thin-sections, see Fig. 6b).

Thermal, hygric and hydric dilatation

The results of thermal cycling show that the thermal deformation is not influenced by the direction of the bedding.

Table 2 Calculated absorption coefficients based on performed measurements

Conservation state	Absorption direction	Absorption coefficient ($g/m^2s^{0.5}$)
Slightly deteriorated	Parallel to the bedding	4–8 ($n = 4$)
Severely deteriorated	Parallel to the bedding	84 ($n = 1$)
	Perpendicular to the bedding	31 ($n = 1$)

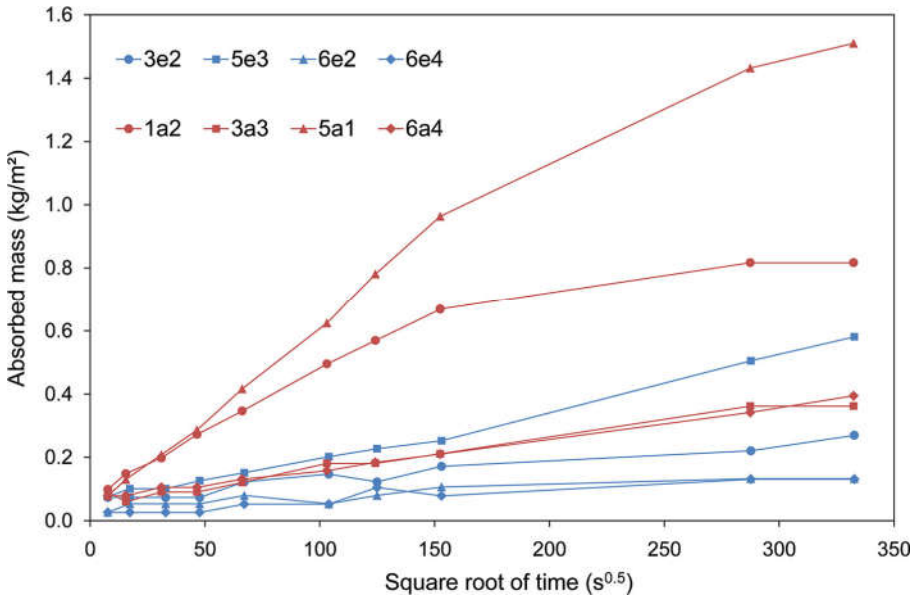

Fig. 9 Capillary absorption *curves* obtained in laboratory conditions. *Red lines* represent capillary uptake parallel to the bedding (code xax); *blue* ones perpendicular to it (code xex) © KIK-IRPA (Monuments Laboratory)

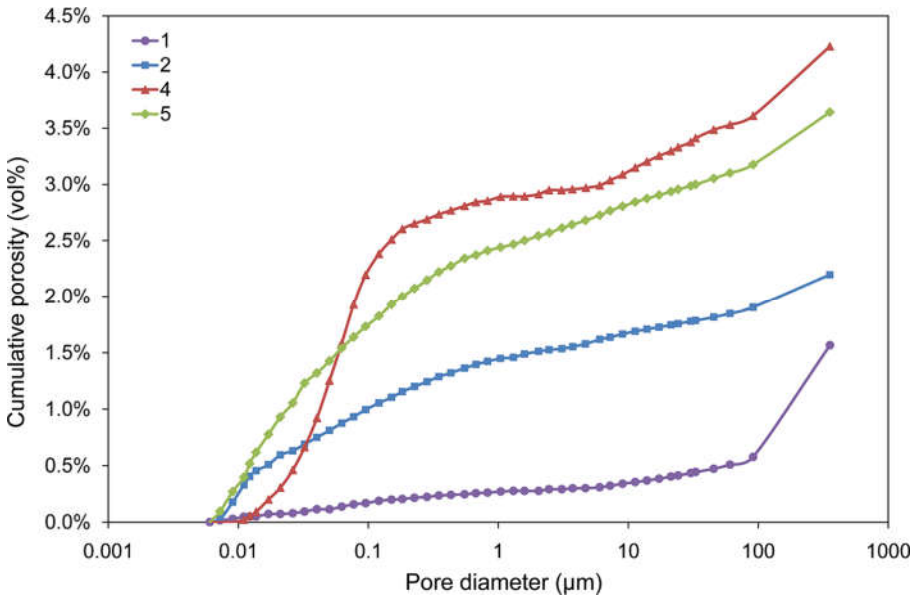

Fig. 10 Cumulative porosity *curves* of 4 samples of Tournai stone © KIK-IRPA (Monuments Laboratory)

The calculated coefficient of thermal expansion of Tournai stone is 5.8×10^{-6}/K (mean value of 4 measurements, 2 per bedding direction), a value in the normal range for sedimentary limestone ($2.85–6.52 \times 10^{-6}$/K) (Siegesmund and Dürrast 2011). The response of the stone to temperature changes is very quick: the delay is not exceeding 10 min.

Figure 11 presents the average dilatation results during RH cycles. It appears that the response of the stone towards changes in RH is delayed by 5 h during the absorption phase, while it is much shorter in the desorption phase. The amplitude is higher in the perpendicular direction and further increases from the first to the second cycle.

Results obtained in case of a hygric shock (from 95 to 40 % RH, at 20 °C) are presented in Fig. 12. Shrinkage in the perpendicular direction ($n = 2$) is much higher than in the parallel direction ($n = 1$). Despite the low number of tests, the findings are in good agreement with the results determined by Lubelli and Nijland (2014) for fresh stone (max ±0.10 %) and, therefore, can be considered as plausible.

Results of hydric expansion by total immersion are presented in Table 3. The numbers reflect the dilatation after 3 days, which corresponds in all cases to a quasi-equilibrium situation (the increase was lower than 0.01 mm/m per hour). The average dilatation

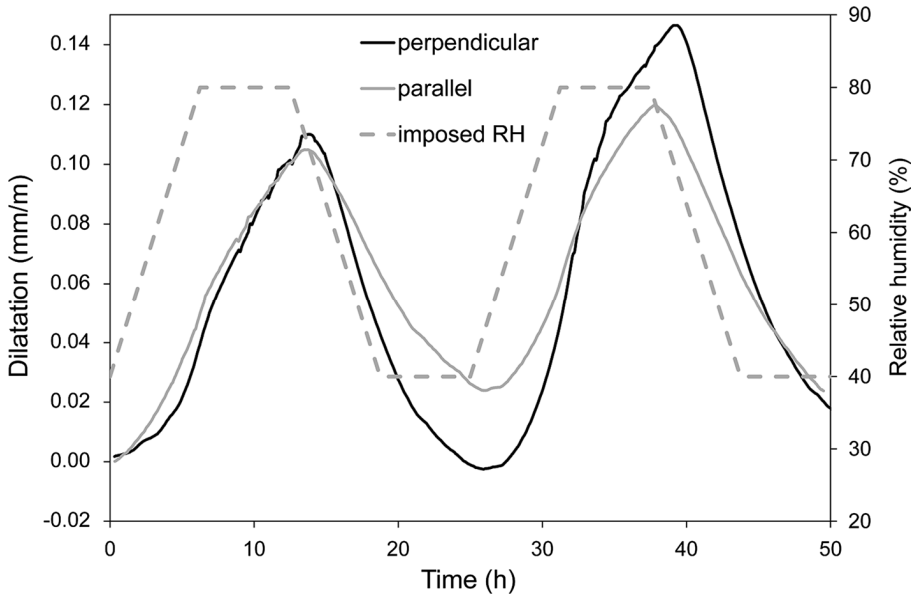

Fig. 11 Dilatation during RH cycles of 40 and 80 % at constant temperature of 20 °C. Average *curves* of 2 measurements for each bedding direction © KIK-IRPA (Monuments Laboratory)

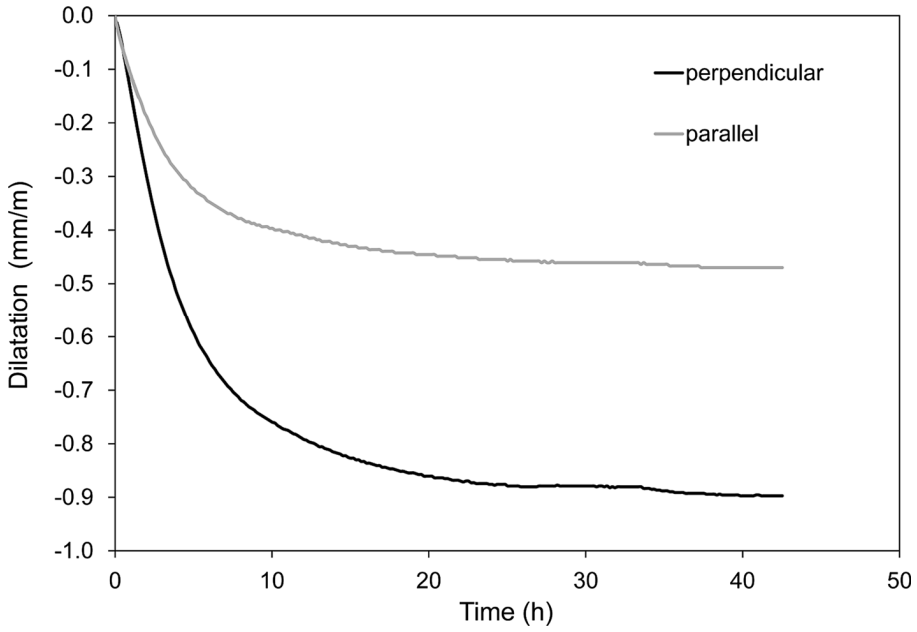

Fig. 12 Hygric shrinkage induced by a hygric shock from 95 to 40 % RH (20 °C). The *black curve* is an average of 2 measurements; the *grey curve* is the result of a single measurement © KIK-IRPA (Monuments Laboratory)

Table 3 Results of hydric dilatation by total immersion after 3 days (72 h)

	Dilatation (mm/m)	
	Perpendicular to the bedding ($n = 4$)	Parallel to the bedding ($n = 5$)
Average	0.97	0.29
Standard deviation	0.28	0.13

perpendicular to the bedding is increased more than threefold compared to the one parallel to the bedding. The absolute values are in the same range as those determined for a hygric shock. When compared to values cited in literature, such values are very high for sedimentary limestone (usual range of 0.02–0.27 mm/m) and can be compared to those for roof slate (0.26–4.80 mm/m) (Siegesmund and Dürrast 2011).

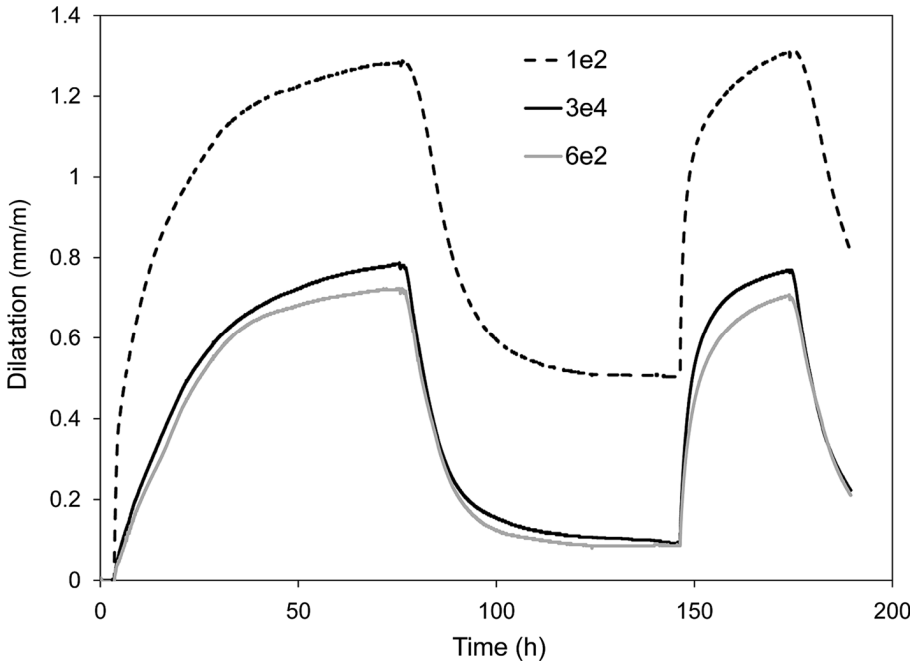

Fig. 13 Dilatation perpendicular to the bedding of 3 samples submitted to hydric cycles. Sample 1e2 cracked during the first water uptake phase © KIK-IRPA (Monuments Laboratory)

Figure 13 shows dilatation results of some samples submitted to 2 cycles, consisting of a wetting phase by immersion ($t = 0$ h) and a drying one in laboratory conditions. The curves illustrate the slowness of the process (3 days are necessary to reach a quasi-equilibrium) and that the deformation is largely reversible, except for sample 1e2. In this particular case, the appearance of a micro-crack at the beginning of the test provoked an irreversible deformation. A similar micro-cracking process induced by water absorption has been observed on other samples. This demonstrates the impact of hydric dilatation on the deterioration process of Tournai stone.

Characterization of the black crusts

The combination of results of optical microscopy and SEM-EDX analyses has allowed identifying a systematic layered structure in the black crusts. Moving from inwards the stone to the surface, the following stratigraphy is observed: (1) stone support; (2) transition zone; (3) superficial crust. However, each of these 3 "layers" displays strong differences depending on whether the crust rather consists of a film or of thick deposits. Microscopic examination suggests that the sulphate source in black crusts is essentially allogenic (resulting from wet and dry deposition) and that the contribution to gypsum formation of finely disseminated pyrite naturally present in black Tournai stone, if any, is supposed to be very limited.

In case crusts are present in the form of rather thin films, the stone support appears relatively sound. Only a few fine micro-cracks can be observed (Fig. 14a). On the other hand, when the crusts have the form of thick deposits, the stone support is always more or less fragmented (Fig. 15). In case of pronounced fragmentation (Fig. 16), gypsum is regularly found between stone flakes where it acts as a micro-crack infill material.

The transition zone is very thin (<250 μm) in the case of films and shows a replacement of the micritic matrix of the stone by gypsum, with the preservation of the original stone fabric (Fig. 14b). Although the lower boundary of the transition zone is diffuse, the upper boundary is characterized by a lack of adhesion, which might correspond to the original stone surface. The mentioned features point out that the stone has been locally transformed into gypsum. Since this replacement of calcite by gypsum has occurred after the initial formation of the stone (genesis), the resulting layer is frequently denominated as "epigen(et)ic" by experts (Bromblet and Vergès-Belmin 1996; Vergès-Belmin and Dignard 2003).

As opposed to the case of films, the transition zone within thick deposits is much thicker: up to several millimetres. It consists of unweathered stone remnants embedded in a weakly cohesive weathered material. Due to the strong fragmentation, the original stone surface is lost.

The superficial crust corresponds to an indurated gypsum layer (Figs. 14c, 15), with entrapped airborne particles, such as fly ashes and very fine quartz grains (<100 μm). The thickness of the superficial crust does not exceed 1 (films) or 2 mm (thick deposits).

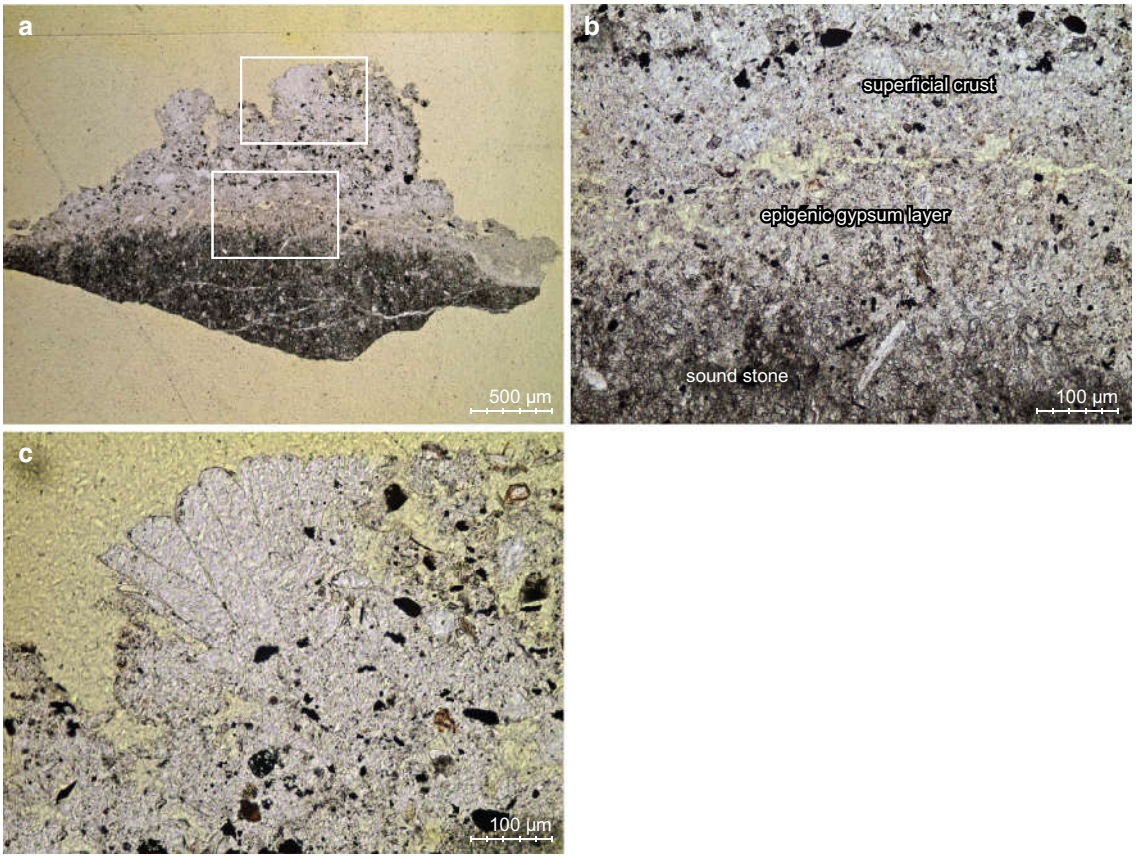

Fig. 14 Thin-section photomicrographs of a film: **a** thin-section overview; **b** zoom on sound stone/epigenic gypsum layer/superficial crust interfaces [*upper marked zone* in (**a**)]; **c** zoom on superficial crust showing opaque particles (fly ashes) and quartz grains embedded in well-developed gypsum crystals [*lower marked zone* in (**a**)] © KIK-IRPA (Monuments Laboratory)

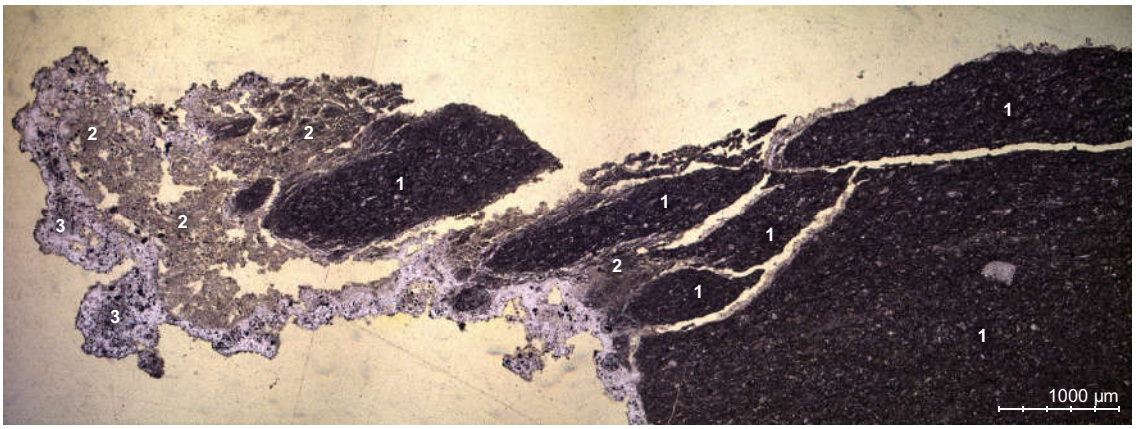

Fig. 15 Sequence of thin-section photomicrographs of thick deposits showing (from the *right* to the *left*): *1* fragmented stone support, *2* weathered stone with stone remnants, and *3* superficial crust © KIK-IRPA (Monuments Laboratory)

Conclusions

Despite its very low porosity and slow absorption rate, water plays an important role in the deterioration pattern of the Tournai stone. It has been demonstrated that hydric and hygric shocks and cycles lead to an important anisotropic deformation of the stone, causing internal shear forces and, when movement is confined, also splitting tensile stresses.

The relative importance of different climatic factors, calculated on expected dilatations on the basis of the

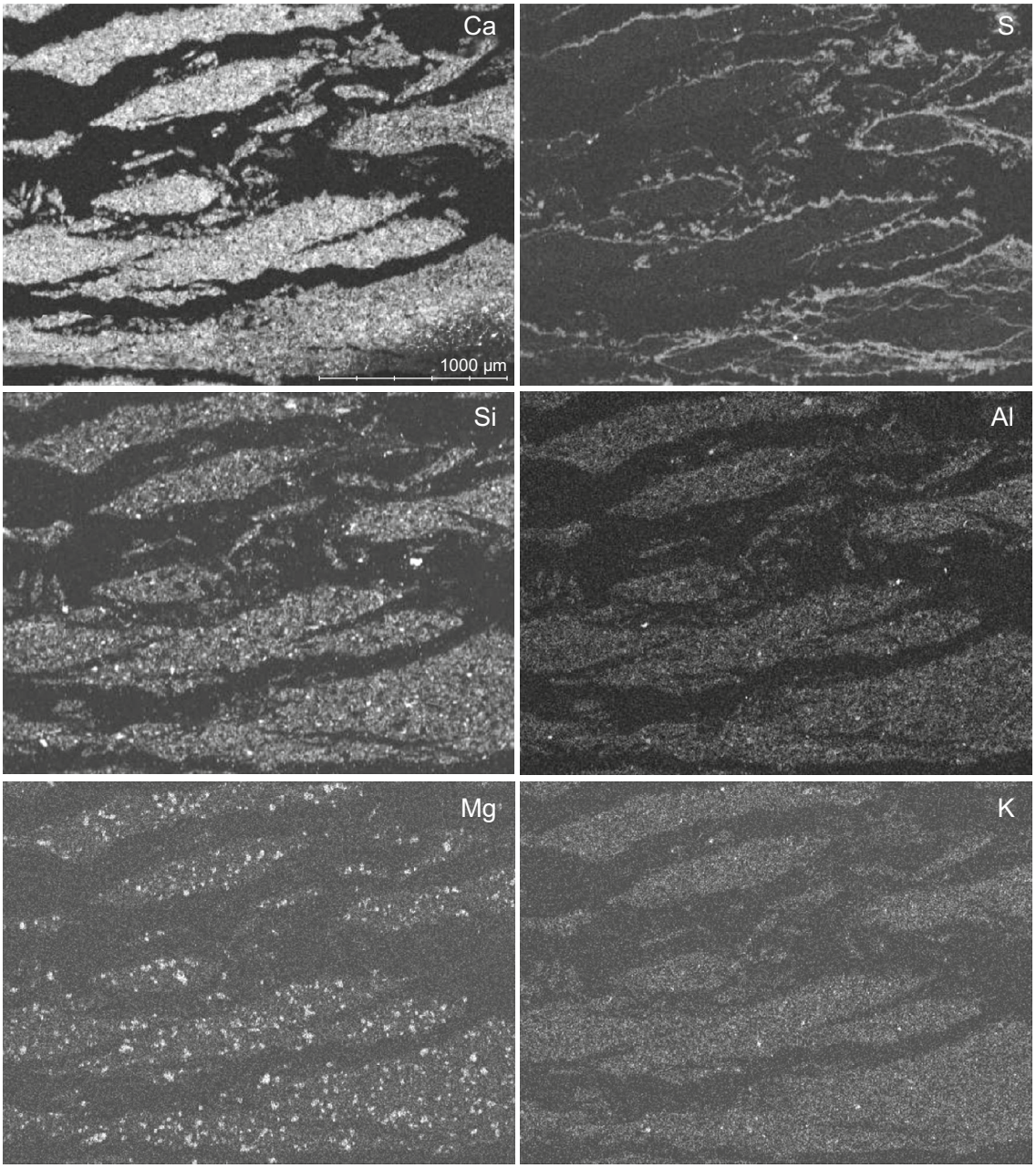

Fig. 16 SEM-EDX mappings of main elements in fragmented stone support. The mapping of calcium gives an overview of the stone flakes, while the one of sulphur indicates that flakes are rimmed with gypsum deposits. The stone flakes are mainly composed of calcite (Ca) and grains of dolomite (Mg–Ca), silica (Si) and illite (Si–Al–K) © KIK-IRPA (Monuments Laboratory)

experimental results and for realistic conditions, is presented in Table 4. Prolonged contact with liquid water (driving rain, runoff and surface condensation) can cause a swelling pressure of nearly the threefold of that resulting from daily relative humidity variations. Daily temperature variations seem to play a subordinate role in the development of swelling pressure. Nevertheless, this pressure might have been significant in the case of the Capitole portal, where direct sun exposure occurred during almost nine centuries.

Even though hygric and hydric deformations are to a large extent reversible processes in the absence of micro-cracks, it is clear that the numerous repetition of cycles over centuries or the pre-existence of micro-cracks—originating for instance from the action of sculpting—can significantly increase the damage potential. Much of the

Table 4 Expected dilatation of Tournai stone caused by various (micro) climatic conditions assumed representative of the portals, determined on the basis of experimental dilatation results during thermal, hygric and hydric cycling

Climatic factor	Expected dilatation perpendicular to bedding (mm/m)	Expected dilatation parallel to bedding (mm/m)
Daily temperature variation (15 °C)	0.06	0.06
Daily RH variation (40 %)	0.14	0.12
Half a day contact with liquid water (12 h)	0.45	0.20

observed damage in the Tournai stone of both portals can be explained by these phenomena.

The actual cause for the swelling on the micro-scale is clearly related to an interaction of water molecules with clay particles. However, since the clay present in the stone, ±8 % on average, consists of a non-swelling clay mineral (illite), intra-crystalline swelling could be ruled out. Nevertheless, another swelling mechanism, though not as much stressed in literature, is related to the presence of clay minerals, referred to as "inter-crystalline" or "inter-particle" osmotic swelling (Ruedrich et al. 2011). This process is driven by the difference in concentration of ions electrostatically attracted to individual clay particles and the ones in the bulk pore water of the rock, causing water ingress in between the particles.

Although freezing conditions were not simulated on water-saturated samples, it is obvious that crystallization of ice in micro-cracks initiated by moisture expansion accelerates the deterioration mechanism by widening and prolonging them. Any existing crack which is connected to the outer surface facilitates deeper water penetration and further deterioration of the stone. Detached stone flakes can, therefore, be considered as being the final result of the combined action of moisture expansion and frost wedging.

Although, gypsum formation cannot be considered as the primary cause of the deterioration, its presence as infill material in-between micro-cracks is not without consequences. Indeed, as it is the case for ice formation, gypsum crystallization exerts pressures that accelerate the deterioration mechanism (Charola et al. 2007). Gypsum infillings, however, might fix the flakes to the stone support which would otherwise have been detached from it.

It is far from evident to propose effective conservation measures for the portals. Most of the damage factors, like the bedding direction of the stone and the likely pre-existence of micro-cracks, cannot be eliminated. Considering the properties of the stone (very low porosity) and of the specificities of the degradation mechanisms (formation of very large micro-cracks), it is very unlikely that consolidation products might completely stop further progressive damage processes. Macro-cracks can be filled with grouts, so that water and vapour transport are slowed down and capillary water is more evenly distributed. Such grouts can be fine-tuned for injectability, colour and physical properties in relation to the stone [see, e.g. the criteria put forward in Snethlage (2011)]. This has been the subject of ample further investigation but falls out of the scope of this paper. Partial results have been presented by R. Hendrickx in the framework of the RILEM TC on non-structural grouts (Lugano 21 May 2014).

Preventive conservation is, however, feasible and it should be concentrated at reducing the exposure to changing environmental conditions and climatic conditions in general, and first of all direct contact with liquid water (driving rain, runoff, condensation and infiltration). Secondly, lowering the amplitude of daily RH and temperature variations will decrease the risk of further damage. Both measures imply sheltering of the portals, either with a relatively simple overhang in open air, or with a closed-off space, in which the climate can be controlled. The question of sheltering seems most relevant for the Mantile portal, which is less exposed and contains the most original sculptures. It would allow avoiding more invasive interventions on the authentic material, such as the entire replacement of the original dripstone. For the case of the Capitole portal, a thorough consideration has to be made as to what effort—and indeed what visual impact—strong conservation measures are justified for the relatively low number of readable sculptures preserved today.

Acknowledgments This research was commissioned by the Walloon cultural heritage agency (*DGO4/Département du Patrimoine*—F. Duperroy), the *Province of Hainaut* and the *City of Tournai*. The results presented here are a part of the preliminary study prior to the restoration of the Mantile and Capitole portals, which has been carried out in collaboration with the Stone Sculpture Workshop of the Royal Institute of Cultural Heritage (KIK-IRPA, Brussels). The authors would like to thank the following colleagues for having contributed to the results presented herein: L. Hoornaert, J. De Roy and C. De Clercq (KIK-IRPA), T. Wangler (ETH Zürich), J. Yans (University of Namur), F. Tourneur (*Pierres et Marbres de Wallonie*), M. Dusar and E. Groessens (Royal Belgian Institute of Natural Sciences).

References

Bromblet P, Vergès-Belmin V (1996) L'élimination des sulfates sur la statuaire calcaire de plein air: une habitude discutable,

Proceedings of Le dessalement des matériaux poreux (7e journées d'étude de la SFIIC), Poitiers (France), May 9–10, pp 55–64

Camerman C (1944) La pierre de Tournai: son gisement, sa structure et ses propriétés, son emploi actuel. Mém Soc Belg Geol, Paléontol et Hydrol, Nouvelle série in-4°, 1, Bruxelles, Belgium. pp 1–86

Charola AE, Pühringer J, Steiger M (2007) Gypsum: a review of its role in the deterioration on building materials. Environ Geol 52:339–352

CSTC (1986) La pierre de Tournai, Annexe 1 de la Note d'Information Technique 163:12

Deléhouzée L (2013) La place des portails dans la chronologie du chantier roman, Book of abstracts Les portails romans de la Cathédrale Notre-Dame de Tournai: Contextualisation et restauration (international conference), Tournai (Belgium), January 31–February 1, p 1

Dingelstadt C, Dreesen R (1996) Atlas pétrographique des principales roches calcaires et roches calcaires gréseuses utilisées dans les monuments de Wallonie (Vol 2). Work commissioned by the Direction Générale de l'Aménagement du Territoire et du Logement, Division des Monuments, Sites et Fouilles, ISSeP, Liège, Belgium, Sheet 10 (Noir de Tournai)

Drake P (2002) The English group of Tournai fonts in the context of the whole school. Ecclesiology Today 29:3–11 (www.ecclsoc.org/ET.29.pdf)

Dunham RJ (1962) Classification of carbonate rocks according to depositional texture. In: Ham WE (ed) Classification of carbonate rocks, Am Assoc Pet Geol Mem 1, pp 108–121

Esquevin J (1969) Influence de la composition chimique des illites sur leur cristallinité. Bull Cent Rech Pau—SNPA 3:147–154

Folk RL (1965) Petrology of sedimentary rocks. Hemphill Publishing Company, Austin (USA) 182 p

Groessens E (2008) La pierre de Tournai: un matériau de choix durant la période romaine et un des fleurons parmi les autres marbres belges. Rev Soc Tournaisienne Geol Prehist et Archeol 10(7):197–216

Hendrickx R (2013) Using the Karsten tube to estimate water transport parameters of porous building materials: the possibilities of analytical and numerical solutions. Mater Struct 46:1309–1320

Hennebert M, Doremus P (1997) Notice explicative de la carte géologique Hertain-Tournai 37/5-6 à l'échelle 1:25000. Direction Générale des Ressources Naturelles et de l'Environnement, Ministère de la Région Wallonne, Jambes, Belgium, p 66

Holtzapffel T (1985) Les minéraux argileux: préparation, analyse diffractométrique et détermination. Soc Geol Nord Publ 12, p 130

ICOMOS-ISCS (2008) Illustrated glossary on stone deterioration patterns—glossaire illustré sur les formes d'altération de la pierre. Monum and Sites XV, p 78

Lubelli B, Nijland TG (2014) Damage mechanism in Tournai limestone—the case of the tomb of admiral tromp in the old church of delft (The Nederlands). J Cult Herit 15(3):313–317

Nys L (1993) La pierre de Tournai: son exploitation et son usage aux XIIIème, XIVème et XVème siècles. Tournai—Louvain-la-Neuve (Tournai—Art et Histoire 8), p 411

RILEM TC 25-PM (1980) Recommended tests to measure the deterioration of stone and to assess the effectiveness of treatments methods. Mater and Struct 13(75):175–253 (in French)

Ruedrich J, Bartelsen T, Dohrmann R, Siegesmund S (2011) Moisture expansion as a deterioration factor for sandstone used in buildings. Environ Earth Sci 63:1545–1564

Siegesmund S, Dürrast H (2011) Physical and mechanical properties of rocks. In: Siegesmund S, Snethlage R (eds) Stone in architecture: properties, durability, 4th edn. Springer, Berlin, pp 97–225

Snethlage R (2011) Stone conservation. In: Siegesmund S, Snethlage R (eds) Stone in architecture: properties, durability, 4th edn. Springer, Berlin, pp 411–544

Storemyr P, Degryse P, King JF (2007) A black Tournai "marble" tombslab from Belgium imported to Trondheim (Norway) in the 12th century: provenance determination based on geological, stylistic and historical evidence. Mater Charact 58:1104–1118

Van Welden J-P (1965) Contribution à l'identification des "Pierres de Tournai". Bull Inst R Patrim Artist 8:149–166

Vergès-Belmin V, Dignard C (2003) Laser yellowing: myth or reality? J Cult Herit 4:238–244